Tensor-Based Compressive Measurements in Two-Dimensional Massive MIMO Systems

Saidur R. Pavel and Yimin D. Zhang
Department of Electrical and Computer Engineering, Temple University, Philadelphia, PA 19122, USA

***Abstract*—This paper considers a massive multiple-input multiple-output (MIMO) system in which the base station is equipped with a uniform rectangular array (URA). To make the practical implementation of such massive MIMO systems feasible, we propose a compressive measurement framework that reduces the dimensionality of the received radio frequency (RF) signals, thereby enabling the use of fewer RF chains and analog-to-digital converters (ADCs) for baseband processing. The framework jointly designs two compressive measurement matrices (CMMs), each corresponding to one spatial dimension, ensuring that the inherent two-dimensional structure of the received signal is preserved. Using the optimized CMMs, we form a reduced-dimensional compressed signal and apply canonical polyadic decomposition (CPD) to the fourth-order covariance tensor to estimate the directions of arrival of the sources.**

***Index Terms*—Direction-of-arrival estimation, uniform rectangular array, massive MIMO, canonical polyadic decomposition**

I. Introduction

Massive multiple-input multiple-output (MIMO) systems equip base stations with a very large number of antennas, offering the potential for orders-of-magnitude improvements in both spectral and energy efficiency through the use of relatively simple linear processing techniques. As a result, massive MIMO is considered a key enabler for future broadband networks that are energy-efficient, spectrally efficient, secure, and robust [1]–[5]. However, the practical implementation of massive MIMO with large-scale antenna arrays faces significant challenges in both hardware design and algorithm development. In particular, fully digital beamforming architectures require each antenna to be connected to a dedicated radio frequency (RF) chain and an analog-to-digital converter (ADC), resulting in a large number of RF front-end circuits. An RF front-end typically consists of a band-pass filter, a low-noise amplifier, a mixer, and a low-pass filter. The need for one RF chain per antenna imposes prohibitive burdens in terms of hardware cost, power consumption, and system complexity, making fully digital processing impractical for massive MIMO deployments. Hybrid analog–digital beamforming has been widely recognized as an effective means to overcome these hardware limitations [6]–[10]. By partitioning the beamforming process into high-dimensional analog processing and low-dimensional digital processing at the baseband, hybrid architectures substantially reduce the number of RF chains needed.

Although many existing studies focus on deploying one-dimensional antenna arrays, particularly uniform linear arrays (ULAs), at the base station of massive MIMO systems, such configurations face practical limitations due to space constraints, especially when accommodating a large number of antenna elements [11]. To overcome the form factor restrictions at the base station and provide two-dimensional (2D) beam steering capability, we consider a 2D antenna arrangement, specifically a uniform rectangular array (URA), in the massive MIMO system. By arranging antenna elements along both the horizontal and vertical dimensions, it becomes feasible to physically accommodate a large number of antennas in a base station. Moreover, a 2D array is required for 2D direction-of-arrival (DOA) estimation and beam steering, which simultaneously captures both the azimuth and elevation angles of a source, offering a more accurate characterization of the signal's spatial properties. As a result, 2D DOA estimation often requires attention for practical source localization applications.

At a given time instant, the received signal at a 2D array is inherently two-dimensional, naturally aligned with the array geometry. When multiple snapshots are collected, the received data becomes a three-dimensional tensor. Traditional signal processing approaches often flatten this high-dimensional signal into a matrix form, thereby losing the inherent multidimensional structure. As a consequence, the spatial and temporal signal characteristics cannot be fully exploited, which may lead to performance degradation [12].

To preserve the tensor structure of the received signal while reducing its dimensionality, we propose optimizing two separate compressive measurement matrices (CMMs), one for each spatial dimension. Optimizing two smaller matrices, rather than a single large one, not only preserves the multidimensional structure of the data but also reduces computational complexity and the number of optimization parameters. Since full-dimensional analog array signals are generally unavailable in practice, the CMMs must be optimized blindly based solely on the compressed digital outputs. To address this, we optimize the CMMs by maximizing the mutual information between the compressed measurements and the signal DOAs, following [13]–[15], which focus linear arrays. Furthermore, recent works [16]–[19] have applied deep learning techniques to optimize the CMMs. In [20], the deep learning-based optimization framework is extended to account for array

This work was supported in part by the National Science Foundation (NSF) under Grant No. ECCS-2236023 and in part by the Air Force Office of Scientific Research (AFOSR) under Grant No. FA9550-23-1-0255.

imperfections in 2D arrays. However, that approach flattens the received signal and its corresponding covariance matrix, thereby losing the original tensor structure.

In this paper, we optimize two CMMs in a massive MIMO system to project the high-dimensional received signal onto a lower-dimensional space while preserving its original multidimensional structure. We then construct a fourth-order covariance tensor and apply canonical polyadic decomposition (CPD) [21], [22] to estimate the steering vectors. The DOA information is then extracted from the estimated steering vectors.

Notations: Lower-case bold letters, upper-case bold letters, and upper-case calligraphic bold letters are used to denote vectors, matrices, and tensors, respectively. Specifically, $\boldsymbol{I}$ and $\boldsymbol{\mathcal{I}}$ represent the identity matrix and the identity tensor of appropriate dimensions, respectively. The operators $(\cdot)^{\mathrm{T}}$, $(\cdot)^*$, and $(\cdot)^{\mathrm{H}}$ denote the transpose, complex conjugate, and Hermitian of a matrix or vector, respectively, while $(\cdot)^\dagger$ denotes the Moore–Penrose pseudoinverse. $\|\cdot\|_{\mathrm{F}}$ denotes the Frobenius norm for tensors or matrices, $[\cdot]_n$ denotes the mode-n unfolding of a tensor, and $\mathrm{vec}(\cdot)$ denotes the vectorization operation. The symbols $\circ$, $\odot$, and $\otimes$ represent the outer product, Hadamard product, and kronceker product, respectively. In addition, $\mathbb{C}^{M\times N}$ denotes the space of $M \times N$ complex-valued matrices, and $\mathbb{E}(\cdot)$ denotes the statistical expectation operator. Finally, $[\cdot]_{\sqcup_i}$ indicates tensor concatenation along the ith dimension, $\times_n$ denotes mode n tensor matrix product, and $\mathcal{A}_1 \overset{i_2}{\underset{i_1}{\times}} \mathcal{A}_2$ denotes the tensor contraction along the i_1th dimension of $\mathcal{A}_1$ and the i_2th dimension of $\mathcal{A}_2$.

CPD: CPD approximates a high-order tensor as a sum of the minimum number of rank-one tensor components. Given an Nth order tensor $\boldsymbol{\mathcal{A}} \in \mathbb{C}^{I_1\times I_2\times\cdots\times I_N}$, its rank-$R$ CPD is formulated as

$$\boldsymbol{\mathcal{A}} = \sum_{r=1}^{R} \eta_r \boldsymbol{a}_1(r)\circ\boldsymbol{a}_2(r)\circ\cdots\circ\boldsymbol{a}_N(r) \triangleq [\![\boldsymbol{\eta}; \boldsymbol{A}_1; \boldsymbol{A}_2; \cdots; \boldsymbol{A}_N]\!], \tag{1}$$

where $\boldsymbol{a}_n(r) \in \mathbb{C}^{I_n}$ represents the rth vector along mode n, and $\boldsymbol{A}_n = [\boldsymbol{a}_n(1), \boldsymbol{a}_n(2), \cdots, \boldsymbol{a}_n(R)] \in \mathbb{C}^{I_n\times R}$ is the factor matrix associated with mode n, for $n = 1, 2, \ldots, N$. The vector $\boldsymbol{\eta} = [\eta_1, \eta_2, \cdots, \eta_R]^{\mathrm{T}}$ contains the scalar weights of the rank-one components.

II. Signal Model

We consider a URA comprising N_x and N_y antennas along the X and Y axes, respectively, as depicted in Fig. 1. The total number of antennas is therefore $N = N_xN_y$. Consider L uncorrelated signals impinging on the massive MIMO system with DOAs $(\boldsymbol{\phi}, \boldsymbol{\theta})$, where $\boldsymbol{\phi} = [\phi_1, \phi_2, \cdots, \phi_L]^{\mathrm{T}}$ and $\boldsymbol{\theta} = [\theta_1, \theta_2, \cdots, \theta_L]^{\mathrm{T}}$ respectively represent the azimuth angles and elevation angles. Defining $\mu_l = \sin(\theta_l)\cos(\phi_l)$ and $\nu_l = \sin(\theta_l)\sin(\phi_l)$, the analog RF signal recived by the antenna array at time t is expressed as

$$\boldsymbol{X}^{\mathrm{RF}}(t) = \sum_{l=1}^{L} s_l(t)e^{j\omega_c t}\boldsymbol{a}(\mu_l)\circ\boldsymbol{a}(\nu_l) + \boldsymbol{N}(t) \in \mathbb{C}^{N_x\times N_y}, \tag{2}$$

where

$$\begin{aligned}\boldsymbol{a}(\mu_l) &= [1, e^{-j\frac{2\pi}{\lambda}d\mu_l}, \cdots, e^{-j\frac{2\pi}{\lambda}(N_x-1)d\mu_l}]^{\mathrm{T}} \in \mathbb{C}^{N_x},\\ \boldsymbol{a}(\nu_l) &= [1, e^{-j\frac{2\pi}{\lambda}d\nu_l}, \cdots, e^{-j\frac{2\pi}{\lambda}(N_x-1)d\nu_l}]^{\mathrm{T}} \in \mathbb{C}^{N_y}\end{aligned} \tag{3}$$

are the steering vectors along the X and Y dimensions corresponding to the DOA (ϕ_l, θ_l), respectively. In addition, $s_l(t)$ denotes the waveform of the lth signal corresponding to DOA (ϕ_l, θ_l), ω_c is the angular frequency of the carrier, and $\boldsymbol{N}(t)$ is a zero-mean additive white Gaussian noise (AWGN) matrix with noise power σ_n^2.

Denote $\boldsymbol{X}(t)$ as the baseband version of the received RF signal $\boldsymbol{X}^{\mathrm{RF}}(t)$. Then, concatenating T snapshots along the temporal dimension results in a three-dimensional received signal tensor, expressed as

$$\begin{aligned}\mathcal{X} &= [\boldsymbol{X}(1), \boldsymbol{X}(2), \cdots, \boldsymbol{X}(T)]_{\sqcup_3}\\ &= \sum_{l=1}^{L} \boldsymbol{a}(\mu_l)\circ\boldsymbol{a}(\nu_l)\circ\boldsymbol{s}_l + \boldsymbol{\mathcal{N}} \in \mathbb{C}^{N_x\times N_y\times T},\end{aligned} \tag{4}$$

where $\boldsymbol{s}_l = [s_l(1), s_l(2), \cdots, s_l(T)]^{\mathrm{T}}$, and $\boldsymbol{\mathcal{N}}$ is the noise tensor.

For massive MIMO with a high number of antennas, dedicating a separate RF chain to each antenna element becomes impractical. To address this, a hybrid analog–digital processing strategy is employed, as illustrated in Fig. 1, where two CMMs, $\boldsymbol{\Phi}_x \in \mathbb{C}^{M_x\times N_x}$ and $\boldsymbol{\Phi}_y \in \mathbb{C}^{M_y\times N_y}$, with $M_x \ll N_x$ and $M_y \ll N_y$, are applied along the X and Y axes, respectively, to preserve the tensor structure of the received signal. Applying these CMMs to the baseband signal $\boldsymbol{X}(t) \in \mathbb{C}^{N_x\times N_y}$ yields a compressed measurement matrix of reduced dimension $M_x \times M_y$, given by

$$\boldsymbol{Y}(t) = \boldsymbol{\Phi}_x\boldsymbol{X}(t)\boldsymbol{\Phi}_y^{\mathrm{H}}. \tag{5}$$

Thus, the number of required RF chains is significantly reduced. After collecting T snapshots, the compressed measurement tensor is expressed as

$$\boldsymbol{\mathcal{Y}} = \boldsymbol{\mathcal{X}} \times_1 \boldsymbol{\Phi}_x \times_2 \boldsymbol{\Phi}_y \in \mathbb{C}^{M_x\times M_y\times T}. \tag{6}$$

The objective is to jointly optimize the CMMs $\boldsymbol{\Phi}_x$ and $\boldsymbol{\Phi}_y$, along with signal DOA estimation based on the compressed array outputs.

III. Optimization of the Compressive Measurement Matrices

Extending from [13]–[15] developed for linear arrays, we consider the DOA (ϕ, θ) as a random variable with a joint probability density function (pdf) $f(\phi, \theta)$. The pdf of the compressed measurement $\boldsymbol{Y}$ is then given as

$$f(\boldsymbol{Y}) = \int_\theta\int_\phi f(\boldsymbol{Y}|\phi, \theta)f(\phi, \theta)\ \mathrm{d}\phi\ \mathrm{d}\theta. \tag{7}$$

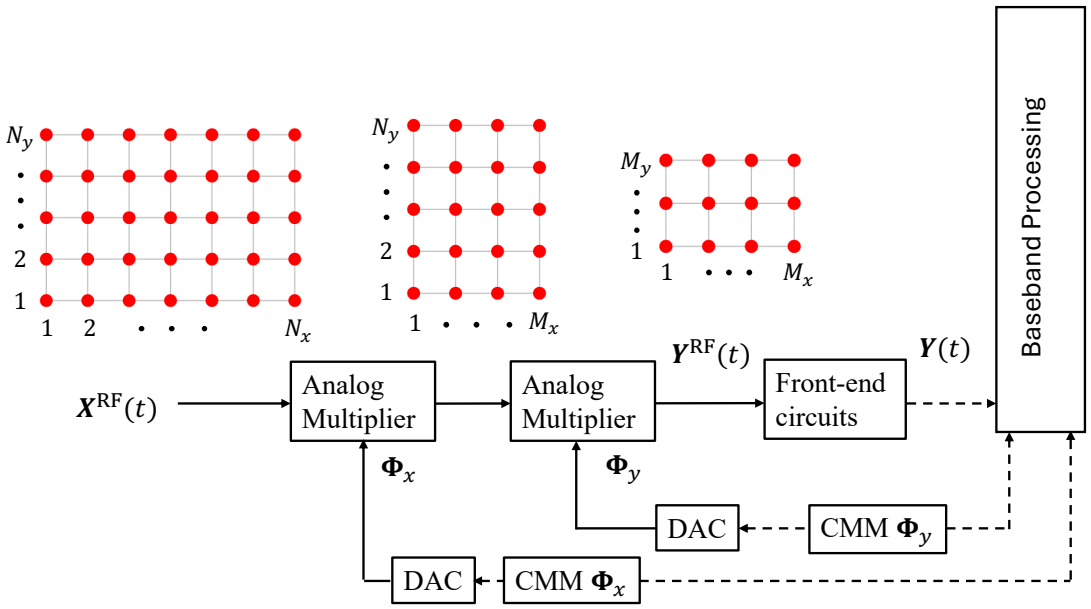

Fig. 1: Compressive measurement framework for 2D array signal.

In the absence of prior knowledge about $f(\phi,\theta)$, we assume that it follows a uniform distribution. The angular domain is discretized into K_x azimuth bins and K_y elevation bins, each with widths $\Delta\phi$ and $\Delta\theta$, respectively. Consequently, the pdf of $\boldsymbol{Y}$ can be approximated as

$$f(\boldsymbol{Y}) = \sum_{k_x=1}^{K_x}\sum_{k_y=1}^{K_y} p_{k_x,k_y} f(\boldsymbol{Y}|\phi,\theta), \tag{8}$$

where $p_{k_x,k_y} = f(\phi,\theta)\Delta\phi\Delta\theta$ denotes the probability of the (k_x,k_y)th angular bin with $\sum_{k_x=1}^{K_x}\sum_{k_y=1}^{K_y} p_{k_x,k_y} = 1$. For a signal impinging from the (k_x,k_y)th angular bin with DOA $(\phi_{k_x},\theta_{k_y})$, the corresponding compressed measurement at time t can be written as

$$\boldsymbol{Y}|\{\phi{=}\phi_{k_x},\theta{=}\theta_{k_y}\} = \boldsymbol{\Phi}_x\left(s(t)\boldsymbol{a}(\mu_{k_x})\circ\boldsymbol{a}(\nu_{k_y}){+}\boldsymbol{N}(t)\right)\boldsymbol{\Phi}_y^{\mathrm{H}}, \tag{9}$$

which follows a matrix Gaussian distribution as

$$\mathrm{vec}(\boldsymbol{Y}) \sim \mathcal{CN}(\boldsymbol{0}, \boldsymbol{C}_{x|k_x,k_y}\otimes\boldsymbol{C}_{y|k_x,k_y}) \tag{10}$$

with covariance matrices for a specific DOA $(\phi_{k_x},\theta_{k_y})$ being

$$\begin{aligned}\boldsymbol{C}_{x|k_x,k_y} &= \boldsymbol{\Phi}_x\left[\sigma_s^2\boldsymbol{a}(\mu_{k_x})\boldsymbol{a}^{\mathrm{H}}(\mu_{k_x}) + \sigma_n^2\boldsymbol{I}\right]\boldsymbol{\Phi}_x^{\mathrm{H}},\\ \boldsymbol{C}_{y|k_x,k_y} &= \boldsymbol{\Phi}_y\left[\sigma_s^2\boldsymbol{a}(\nu_{k_y})\boldsymbol{a}^{\mathrm{H}}(\nu_{k_y}) + \sigma_n^2\boldsymbol{I}\right]\boldsymbol{\Phi}_y^{\mathrm{H}},\end{aligned} \tag{11}$$

along the X and Y axes, respectively.

We then optimize the CMMs $\boldsymbol{\Phi}_x$ and $\boldsymbol{\Phi}_y$ by maximizing mutual information of the compressed measurement and the signal DOAs in a gradient ascent startegy, expressed as

$$\begin{aligned}\boldsymbol{\Phi}_x &\leftarrow \boldsymbol{\Phi}_x + \gamma\nabla_{\boldsymbol{\Phi}_x} I(\boldsymbol{Y};\phi,\theta),\\ \boldsymbol{\Phi}_y &\leftarrow \boldsymbol{\Phi}_y + \gamma\nabla_{\boldsymbol{\Phi}_y} I(\boldsymbol{Y};\phi,\theta),\end{aligned} \tag{12}$$

where $\nabla_{\boldsymbol{\Phi}_x}\{\cdot\}$ and $\nabla_{\boldsymbol{\Phi}_y}\{\cdot\}$ are the gradient operators with respect to $\boldsymbol{\Phi}_x$ and $\boldsymbol{\Phi}_y$, respectively. The gradients of mutual information can be derived as

$$\begin{aligned}&\nabla_{\boldsymbol{\Phi}_x} I(\boldsymbol{Y};\theta)\\ &= \frac{\sum_{k_x=1}^{K_x}\sum_{k_y=1}^{K_y} p_{k_x,k_y}\frac{\boldsymbol{D}^{-1}_{x_{k_x,k_y}}}{|\boldsymbol{D}_{x_{k_x,k_y}}|}\boldsymbol{\Phi}_x\boldsymbol{E}_{x_{k_x,k_y}}}{\sum_{k_x=1}^{K_x}\sum_{k_y=1}^{K_y} p_{k_x,k_y}|\boldsymbol{D}_{x_{k_x,k_y}}|^{-1}}\\ &- \sum_{k_x=1}^{K_x}\sum_{k_y=1}^{K_y} p_{k_x,k_y}\boldsymbol{E}_{x_{k_x,k_y}}\end{aligned} \tag{13}$$

and

$$\begin{aligned}&\nabla_{\boldsymbol{\Phi}_y} I(\boldsymbol{Y};\theta)\\ &= \frac{\sum_{k_x=1}^{K_x}\sum_{k_y=1}^{K_y} p_{k_x,k_y}\frac{\boldsymbol{D}^{-1}_{y_{k_x,k_y}}}{|\boldsymbol{D}_{y_{k_x,k_y}}|}\boldsymbol{\Phi}_y\boldsymbol{E}_{y_{k_x,k_y}}}{\sum_{k_x=1}^{K_x}\sum_{k_y=1}^{K_y} p_{k_x,k_y}|\boldsymbol{D}_{y_{k_x,k_y}}|^{-1}}\\ &- \sum_{k_x=1}^{K_x}\sum_{k_y=1}^{K_y} p_{k_x,k_y}\boldsymbol{E}_{y_{k_x,k_y}},\end{aligned} \tag{14}$$

respectively, where

$$\begin{aligned}\boldsymbol{E}_{x_{k_x,k_y}} &= \frac{\sigma_s^2}{\sigma_n^2}\boldsymbol{a}(\mu_{k_x})\boldsymbol{a}^{\mathrm{H}}(\mu_{k_x}) + \boldsymbol{I},\\ \boldsymbol{E}_{y_{k_x,k_y}} &= \frac{\sigma_s^2}{\sigma_n^2}\boldsymbol{a}(\nu_{k_y})\boldsymbol{a}^{\mathrm{H}}(\nu_{k_y}) + \boldsymbol{I},\end{aligned} \tag{15}$$

$\boldsymbol{D}_{x_{k_x,k_y}} = \sigma_n^{-2}\boldsymbol{C}_{x|k_x,k_y}$, and $\boldsymbol{D}_{y_{k_x,k_y}} = \sigma_n^{-2}\boldsymbol{C}_{y|k_x,k_y}$.

We impose a row-orthonormality constraint on $\boldsymbol{\Phi}_x$ and $\boldsymbol{\Phi}_y$, i.e., $\boldsymbol{\Phi}_x\boldsymbol{\Phi}_x^{\mathrm{H}} = \boldsymbol{I}$ and $\boldsymbol{\Phi}_y\boldsymbol{\Phi}_y^{\mathrm{H}} = \boldsymbol{I}$, to ensure that scaling by $\boldsymbol{\Phi}_x$ and $\boldsymbol{\Phi}_y$ does not increase the mutual information. Moreover, the elements of $\boldsymbol{\Phi}_x$ and $\boldsymbol{\Phi}_y$ are normalized to constant modulus, facilitating implementation with phase shifters.

Once we obtain optimized $\boldsymbol{\Phi}_x$ and $\boldsymbol{\Phi}_y$, the compressed measurement tensor $\boldsymbol{\mathcal{Y}}$ is obtained as

$$\boldsymbol{\mathcal{Y}} = \boldsymbol{\mathcal{X}} \times_1 \boldsymbol{\Phi}_x \times_2 \boldsymbol{\Phi}_y, \tag{16}$$

and the fourth-order covariance tensor of the compressed measurement tensor becomes

$$\begin{aligned} \boldsymbol{\mathcal{R}}_{\boldsymbol{\mathcal{Y}}} &= \mathbb{E}[\boldsymbol{Y}(t) \circ \boldsymbol{Y}^*(t)] \\ &= \sum_{l=1}^{L} \sigma_l^2 \boldsymbol{\Phi}_x \boldsymbol{a}(\mu_l) \circ \boldsymbol{\Phi}_y \boldsymbol{a}(\nu_l) \\ &\quad \circ \boldsymbol{\Phi}_x^* \boldsymbol{a}(\mu_l)^* \circ \boldsymbol{\Phi}_y^* \boldsymbol{a}(\nu_l)^* + \boldsymbol{\mathcal{N}}. \end{aligned} \tag{17}$$

In practice, the sample covariance tensor can be computed as

$$\hat{\boldsymbol{\mathcal{R}}}_y = \frac{1}{T} \boldsymbol{\mathcal{Y}} \overset{3}{\times}_3 \boldsymbol{\mathcal{Y}}^*. \tag{18}$$

Since the CMMs $\boldsymbol{\Phi}_x$ and $\boldsymbol{\Phi}_y$ are initially optimized assuming a uniform DOA prior, the resulting estimate may not accurate. To refine the prior, the estimated covariance tensor $\hat{\mathcal{R}}_y$ is reshaped into a matrix, and the spatial spectrum is computed using the minimum variance distortionless response (MVDR) method. The normalized spectrum is then used as an updated DOA prior, and the CMMs are re-optimized accordingly.

IV. CPD-BASED DOA ESTIMATION

A. Estimation of the Factor Matrices

Eq. (17) admits a rank-L canonical polyadic problem, and the covariance tensor can be decomposed via CPD to obtain the factor matrices as

$$\begin{aligned} \hat{\boldsymbol{G}}_x &= [(\boldsymbol{\Phi}_x \boldsymbol{a}(\mu_1)), \cdots, (\boldsymbol{\Phi}_x \boldsymbol{a}(\mu_L))] \in \mathbb{C}^{M_x \times L}, \\ \hat{\boldsymbol{G}}_y &= [(\boldsymbol{\Phi}_y \boldsymbol{a}(\nu_1)), \cdots, (\boldsymbol{\Phi}_y \boldsymbol{a}(\nu_L))] \in \mathbb{C}^{M_y \times L}. \end{aligned} \tag{19}$$

More specifically, the CPD of $\hat{\boldsymbol{\mathcal{R}}}_y$ can be obtained from the following least squares optimization problem [23]

$$\left\{ \hat{\boldsymbol{G}}_x, \hat{\boldsymbol{G}}_y \right\} = \arg \min_{\hat{\boldsymbol{G}}_x, \hat{\boldsymbol{G}}_y} \left\| \hat{\boldsymbol{\mathcal{R}}}_y - [\![\boldsymbol{\eta}; \hat{\boldsymbol{G}}_x, \hat{\boldsymbol{G}}_y, \hat{\boldsymbol{G}}_x^*, \hat{\boldsymbol{G}}_y^*]\!] \right\|_{\mathrm{F}}^2. \tag{20}$$

The least squares problem defined in Eq. (20) can be solved by iteratively updating the factor matrices $\hat{\boldsymbol{G}}_x$ and $\hat{\boldsymbol{G}}_y$ as

$$\begin{aligned} \hat{\boldsymbol{G}}_x &= \arg \min_{\hat{\boldsymbol{G}}_x} \left\| [\hat{\boldsymbol{\mathcal{R}}}_y]_1 - \hat{\boldsymbol{G}}_x \left(\hat{\boldsymbol{G}}_y^* \odot \hat{\boldsymbol{G}}_x^* \odot \hat{\boldsymbol{G}}_y \right)^{\mathrm{T}} \right\|_{\mathrm{F}}^2, \\ \hat{\boldsymbol{G}}_y &= \arg \min_{\hat{\boldsymbol{G}}_y} \left\| [\hat{\boldsymbol{\mathcal{R}}}_y]_2 - \hat{\boldsymbol{G}}_y \left(\hat{\boldsymbol{G}}_y^* \odot \hat{\boldsymbol{G}}_x^* \odot \hat{\boldsymbol{G}}_x \right)^{\mathrm{T}} \right\|_{\mathrm{F}}^2. \end{aligned} \tag{21}$$

At each iteration the closed-form solution is obtained as

$$\begin{aligned} \hat{\boldsymbol{G}}_x &= [\hat{\boldsymbol{\mathcal{R}}}_y]_1 \left[\left(\hat{\boldsymbol{G}}_y^* \odot \hat{\boldsymbol{G}}_x^* \odot \hat{\boldsymbol{G}}_y \right)^{\mathrm{T}} \right]^{\dagger}, \\ \hat{\boldsymbol{G}}_y &= [\hat{\boldsymbol{\mathcal{R}}}_y]_2 \left[\left(\hat{\boldsymbol{G}}_y^* \odot \hat{\boldsymbol{G}}_x^* \odot \hat{\boldsymbol{G}}_x \right)^{\mathrm{T}} \right]^{\dagger}. \end{aligned} \tag{22}$$

The iterations continue until the relative error in the decomposed covariance tensor between consecutive steps falls below a predefined convergence threshold. Note that, to ensure unique identifiability of the CPD factor matrices, the number of sources L should satisfy $L \leq M_x + M_y - 2$.

B. DOA Estimation

Denote the columns of the estimated CPD factor matrices as $\boldsymbol{b}_k$ and $\boldsymbol{c}_k$, respectively, such that $\hat{\boldsymbol{G}}_x = [\boldsymbol{b}_1, \cdots, \boldsymbol{b}_L]$ and $\hat{\boldsymbol{G}}_y = [\boldsymbol{c}_1, \cdots, \boldsymbol{c}_L]$. Then, μ_l and ν_l are estimated as

$$\begin{aligned} \hat{\mu}_l &= \arg \max_{\mu_l} \boldsymbol{a}^{\mathrm{H}}(\mu_l) \boldsymbol{\Phi}_x^{\mathrm{H}} \boldsymbol{b}_l, \\ \hat{\nu}_l &= \arg \max_{\nu_l} \boldsymbol{a}^{\mathrm{H}}(\nu_l) \boldsymbol{\Phi}_y^{\mathrm{H}} \boldsymbol{c}_l. \end{aligned} \tag{23}$$

Once $\hat{\mu}_l$ and $\hat{\nu}_l$ are obtained, the azimuth and elevation angles for the lth signal are respectively estimated as

$$\begin{aligned} \hat{\phi}_l &= \arctan\left(\frac{\hat{\nu}_l}{\hat{\mu}_l} \right), \\ \hat{\theta}_l &= \arcsin\left(\sqrt{\hat{\mu}_l^2 + \hat{\nu}_l^2} \right). \end{aligned} \tag{24}$$

V. SIMULATION RESULTS

We consider a massive MIMO system where $N = 100$ receive antennas are arranged in a uniform rectangular fashion with $(N_x, N_y) = (10, 10)$. The size of the CMMs, i.e., $\boldsymbol{\Phi}_x$ and $\boldsymbol{\Phi}_y$, are both 5×10, resulting in a compressed measurement of size $(M_x, M_y) = (5, 5)$. Therefore, the compression ratio is $\frac{N_x N_y}{M_x M_y} = 4$. The DOA pdf is discretized with an angular resolution of $\Delta\phi = \Delta\theta = 0.5^\circ$. We perform 50 inner iterations of gradient ascent to optimize the CMMs for a given DOA prior, using a step size of 0.1, and 3 outer iterations with the updated DOA prior. We consider 7 uncorrelated signals with azimuth angles 15°, -55°, -30°, -20°, 10°, 25°, and 35°, and corresponding elevation angles 60°, 35°, 5°, 55°, 20°, 50°, and 25°. The input SNR is 10 dB, and 1,000 snapshots are considered.

Fig. 2 illustrates the DOA estimation results obtained from the compressed covariance tensor across successive outer iterations. As shown in Fig. 2(a), in the first outer iteration where a uniform DOA prior is assumed, a noticeable estimation error occurs for one of the signals. However, as the number of outer iterations increases, the estimates improve. For instance, by the third outer iteration shown in Fig. 2(c), the estimated DOAs converge closely to their true values.

VI. CONCLUSION

In this paper, we developed an effective compression framework for high-dimensional analog received signals in a massive MIMO system, where the base station is equipped with a URA. Two CMMs are optimized, one for each spatial dimension, in order to preserve the structural characteristics of the received signal. The optimization was performed by maximizing the mutual information between the compressed measurements and the signal DOAs. To exploit this preserved structure, CPD was applied to the compressed covariance tensor to estimate the DOAs. The proposed iterative optimization scheme successfully improved the CMMs, enabling accurate DOA estimation from compressed data, as demonstrated by the simulation results.

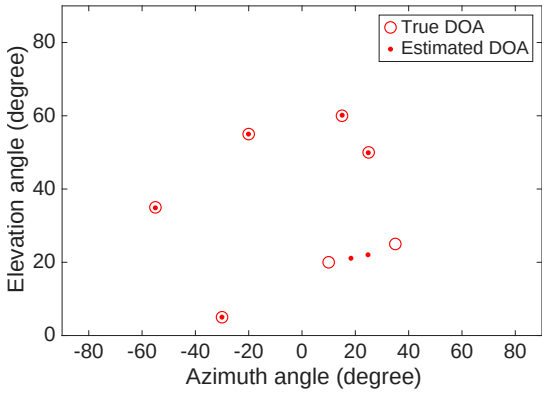

(a) Outer iteration 1

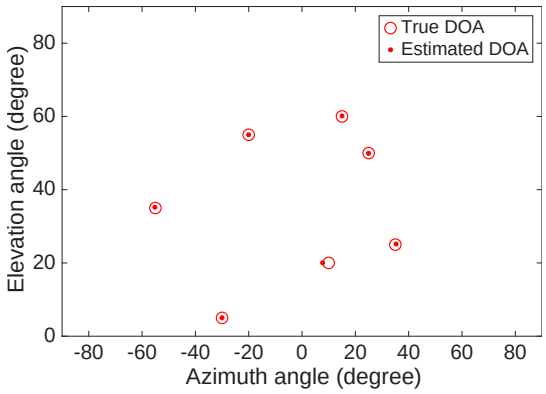

(b) Outer iteration 2

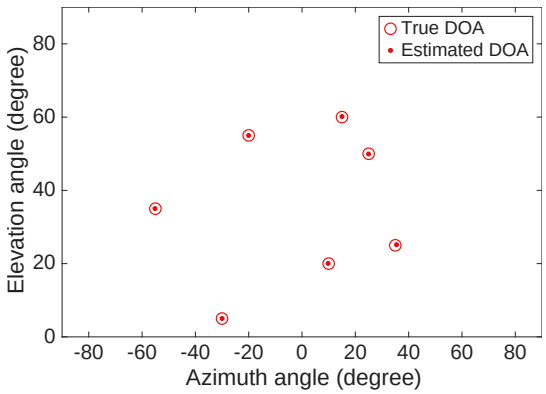

(c) Outer iteration 3

Fig. 2: Estimated DOAs in the first three iterations.

REFERENCES

[1] F. Rusek, D. Persson, B. K. Lau, E. G. Larsson, T. L. Marzetta, O. Edfors, and F. Tufvesson, "Scaling up MIMO: Opportunities and challenges with very large arrays," *IEEE Signal Process. Mag.*, vol. 30, no. 1, pp. 40–60, 2012.

[2] E. G. Larsson, O. Edfors, F. Tufvesson, and T. L. Marzetta, "Massive MIMO for next generation wireless systems," *IEEE Commun. Mag.*, vol. 52, no. 2, pp. 186–195, 2014.

[3] L. Lu, G. Y. Li, A. L. Swindlehurst, A. Ashikhmin, and R. Zhang, "An overview of massive MIMO: Benefits and challenges," *IEEE J. Sel. Top. Signal Process.*, vol. 8, no. 5, pp. 742–758, 2014.

[4] F. Jiang, J. Chen, A. L. Swindlehurst, and J. A. López-Salcedo, "Massive MIMO for wireless sensing with a coherent multiple access channel," *IEEE Trans. Signal Process.*, vol. 63, no. 12, pp. 3005–3017, 2015.

[5] A. Alkhateeb, O. El Ayach, G. Leus, and R. W. Heath, "Channel estimation and hybrid precoding for millimeter wave cellular systems," *IEEE J. Sel. Top. Signal Process.*, vol. 8, no. 5, pp. 831–846, 2014.

[6] X. Wu, D. Liu, and F. Yin, "Hybrid beamforming for multi-user massive mimo systems," *IEEE Trans. Commun.*, vol. 66, no. 9, pp. 3879–3891, 2018.

[7] M. Guo, Y. D. Zhang, and T. Chen, "DOA estimation using compressed sparse array," *IEEE Trans. Signal Process.*, vol. 66, no. 15, pp. 4133–4146, 2018.

[8] I. Ahmed, H. Khammari, A. Shahid, A. Musa, K. S. Kim, E. De Poorter, and I. Moerman, "A survey on hybrid beamforming techniques in 5G: Architecture and system model perspectives," *IEEE Commun. Surveys & Tutorials*, vol. 20, no. 4, pp. 3060–3097, 2018.

[9] T. Lin, J. Cong, Y. Zhu, J. Zhang, and K. B. Letaief, "Hybrid beamforming for millimeter wave systems using the MMSE criterion," *IEEE Trans. Commun.*, vol. 67, no. 5, pp. 3693–3708, 2019.

[10] J. Zhang, X. Yu, and K. B. Letaief, "Hybrid beamforming for 5G and beyond millimeter-wave systems: A holistic view," *IEEE Open J. Commun. Soc.*, vol. 1, pp. 77–91, 2019.

[11] A. Wang, L. Liu, and J. Zhang, "Low complexity direction of arrival (DOA) estimation for 2d massive MIMO systems," in *Proc. IEEE Globecom Workshops*. IEEE, 2012, pp. 703–707.

[12] H. Zheng, C. Zhou, Z. Shi, Y. Gu, and Y. D. Zhang, "Coarray tensor direction-of-arrival estimation," *IEEE Trans. Signal Process.*, vol. 71, pp. 1128–1142, 2023.

[13] Y. Gu, Y. D. Zhang, and N. A. Goodman, "Optimized compressive sensing-based direction-of-arrival estimation in massive MIMO," in *Proc. IEEE Int. Conf. Acoust. Speech Signal Process. (ICASSP)*, New Orleans, LA, March 2017, pp. 3181–3185.

[14] Y. Gu and Y. D. Zhang, "Compressive sampling optimization for user signal parameter estimation in massive MIMO systems," *Digital Signal Process.*, vol. 94, pp. 105–113, 2019.

[15] Y. D. Zhang, "Iterative learning for optimized compressive measurements in massive MIMO systems," in *Proc. IEEE Radar Conf.*, New York, NY, 2022, pp. 1–5.

[16] S. R. Pavel, Y. D. Zhang, M. S. Greco, and F. Gini, "Deep learning-based compressive sampling optimization in massive MIMO systems," in *Proc. IEEE Int. Conf. Acoust. Speech Signal Process. (ICASSP)*, Rhodes Island, Greece, June 2023, pp. 1–5.

[17] S. R. Pavel and Y. D. Zhang, "Optimization of the compressive measurement matrix in a massive MIMO system exploiting LSTM networks," *Algorithms*, vol. 16, no. 261, pp. 1–16, 2023.

[18] M. S. R. Pavel and Y. D. Zhang, "Deep learning-based robust imaging exploiting 2-D array compressive measurement," in *Proc. Asilomar Conf. Signals, Systems, and Computers*, Pacific Grove, CA, Oct. 2022, pp. 1433–1437.

[19] F. Sohrabi, Z. Chen, and W. Yu, "Deep active learning approach to adaptive beamforming for mmWave initial alignment," *IEEE J. Sel. Areas Commun.*, vol. 39, no. 8, pp. 2347–2360, 2021.

[20] S. R. Pavel and Y. D. Zhang, "Neural network approach to iterative optimization of compressive measurement matrix in massive MIMO system," in *Proc. IEEE Sensor Array and Multichannel Signal Processing Workshop (SAM)*, Trondheim, Norway, June 2022, pp. 171–175.

[21] J. D. Carroll and J.-J. Chang, "Analysis of individual differences in multidimensional scaling via an N-way generalization of 'Eckart-Young' decomposition," *Psychometrika*, vol. 35, no. 3, pp. 283–319, 1970.

[22] R. A. Harshman, "Foundations of the PARAFAC procedure: Models and conditions for an 'explanatory' multimodal factor analysis," *UCLA Work. Papers Phonetics*, vol. 16, pp. 1–84, 1970.

[23] N. D. Sidiropoulos, L. De Lathauwer, X. Fu, K. Huang, E. E. Papalexakis, and C. Faloutsos, "Tensor decomposition for signal processing and machine learning," *IEEE Trans. Signal Process.*, vol. 65, no. 13, pp. 3551–3582, 2017.